



Case Report

Prometastatic CXCR4 and Histone Methyltransferase EZH2 Are Upregulated in *SMARCB1/INI1*-Deficient and *TP53*-Mutated Poorly Differentiated Chordoma

Albina Joldoshova ^{1,*} , Shaimaa Elzamy ², Robert Brown ² and Jamie Buryanek ^{2,*}

¹ Department of Pathology and Immunology, Baylor College of Medicine, Houston, TX 77030, USA

² Department of Pathology and Laboratory Medicine, The University of Texas Health Science Center at Houston, McGovern Medical School, Houston, TX 77030, USA

* Correspondence: albina.joldoshova@bcm.edu (A.J.); jamie.buryanek@uth.tmc.edu (J.B.)

Abstract: Background: Chordoma is a rare tumor most commonly arising in the sacrococcygeal region from notochord remnants. Usually, these tumors are locally invasive and recurrent, and they have a 5–43% ability to metastasize. A newly-described aggressive variant called poorly differentiated chordoma is different from conventional chordoma in that it does not have the well-differentiated histologic appearance of conventional chordoma and also exhibits the loss of *SMARCB1/INI1*. Herein, we describe a case of poorly differentiated chordoma with *SMARCB1/INI1* loss, a concurrent *TP53* mutation, and *Rb1* loss. Methods: The patient is a middle-aged man with a history of previously resected sacrococcygeal chordoma, who was found to have new hepatic, lung, and adrenal lesions. Results: Biopsy of the liver lesion showed sheets of malignant epithelioid cells with vacuolated cytoplasm, areas of necrosis, and up to five mitoses in one high-power field. No physaliferous cytologic features or matrix material was seen. After reviewing an extensive panel of immunohistochemical markers, the origin of the metastatic tumor could not be determined; the tumor was only positive for Cam5.2, EMA, and CD56. Brachyury was performed due to the patient's previous history and was positive. Genomic testing showed a *SMARCB1* mutation, *TP53* mutation, and *RB1* loss. Additional markers were performed, and the tumor showed a Ki-67 proliferation index of approximately 80%, mutant p53 protein, loss of *INI1*, and strong expression of both the histone methyl transferase *EZH2* and the chemokine receptor *CXCR4*. Conclusions: Poorly differentiated chordoma is a highly aggressive variant of chordoma with few cases reported. This case of *SMARCB1/INI1*-deficient, poorly differentiated chordoma also showed a concurrent *TP53* mutation and loss of *RB1*, which resulted in malignant transformation with upregulation of both prometastatic *CXCR4* and the histone methyltransferase *EZH2*, causing aggressive behavior and metastasis.



Citation: Joldoshova, A.; Elzamy, S.; Brown, R.; Buryanek, J. Prometastatic CXCR4 and Histone Methyltransferase EZH2 Are Upregulated in *SMARCB1/INI1*-Deficient and *TP53*-Mutated Poorly Differentiated Chordoma. *J. Mol. Pathol.* **2022**, *3*, 68–77. <https://doi.org/10.3390/jmp3020007>

Academic Editor: Giancarlo Troncone

Received: 5 January 2022

Accepted: 28 March 2022

Published: 2 April 2022

Publisher's Note: MDPI stays neutral with regard to jurisdictional claims in published maps and institutional affiliations.



Copyright: © 2022 by the authors. Licensee MDPI, Basel, Switzerland. This article is an open access article distributed under the terms and conditions of the Creative Commons Attribution (CC BY) license (<https://creativecommons.org/licenses/by/4.0/>).

Keywords: poorly differentiated chordoma 1; *EZH2* 2; *CXCR4* 3

1. Introduction

Chordoma is a rare tumor most commonly arising in the sacrococcygeal region from notochord remnants [1]. Usually, these tumors are locally invasive and recurrent, and they have a wide range (<5–43%) of capacity to metastasize, such as to the skin, lungs, and bone [2]. A newly-described aggressive variant called poorly differentiated chordoma is different from conventional chordoma in that it does not have the well-differentiated histologic appearance of conventional chordoma and exhibits loss of *SMARCB1/INI1* [3]. Herein, we describe a case of poorly differentiated chordoma with *SMARCB1/INI1* loss, concurrent with a *TP53* mutation and *Rb1* loss, which has never been reported in the literature to the best of our knowledge.

Let us explore the pathogenetic changes that occur and the resulting consequences on the pathobiology of the tumor to allow for this especially aggressively behaving variant of chordoma [4]. *SMARCB1* (codes for *INI1*) is a component of the SWItch/Sucrose

Non-Fermentable Complex (SWI/SNF) and is expressed in all cell types. The SWI/SNF complex functions as a tumor suppressor and is involved in chromatin remodeling and transcriptional regulation [4,5]. If any of the subunits (such as INI1) are lost due to mutation, the SWI/SNF complex cannot assemble, and the tumor suppressor function of this large complex is lost [6]. Loss of SWI/SNF and its normal tumor suppressive function leads to elevated expression of enhancer of zeste homolog 2 (EZH2). EZH2 is a histone methyltransferase that induces stemness in tumors by causing proliferation at the expense of differentiation and functions that repress tumor suppressor genes [7]. This upregulation in EZH2 occurs because there is normally epigenetic antagonism between the SWI/SNF tumor suppressor complex and EZH2 [8]. Loss of SWI/SNF can also lead to deregulation of the C-X-C chemokine receptor type 4 (CXCR4) pathway, which was demonstrated in the atypical teratoid/rhabdoid tumor (AT/RT) [9]. CXCR4 is a receptor in the chemokine family that, when stimulated by its ligand, stromal-derived factor-1 (SDF-1/CXCL12), induces downstream signaling to promote cell proliferation and metastasis in tumors [10]. Furthermore, EZH2 can also cause upregulation of prometastatic CXCR4 by repressing tumor-suppressive microRNAs (i.e., miR-622 and miR-9) [11,12].

Like INI1, the p53 protein has tumor-suppressive functions, and its mutation can cause changes in chordoma related to malignant transformation. Mutant p53 induces EZH2 expression and epithelial-mesenchymal transition (EMT) due to the attenuation of miR-26a processing [13]. Normally, wild-type p53 suppresses CXCR4 expression. Naturally, loss of this tumor-suppressive function would cause an increase in CXCR4. In a study of breast cancer cell lines, it was shown that the loss of functional p53 resulted in a 10-fold increase in CXCR4 [14]. Finally, the loss of Rb1 results in loss of cell cycle regulation and progression through the cell cycle [15]. Please refer to Figure 1 for graphical illustration of the INI1, EZH2, CXCR4, and mutant TP53 interaction.

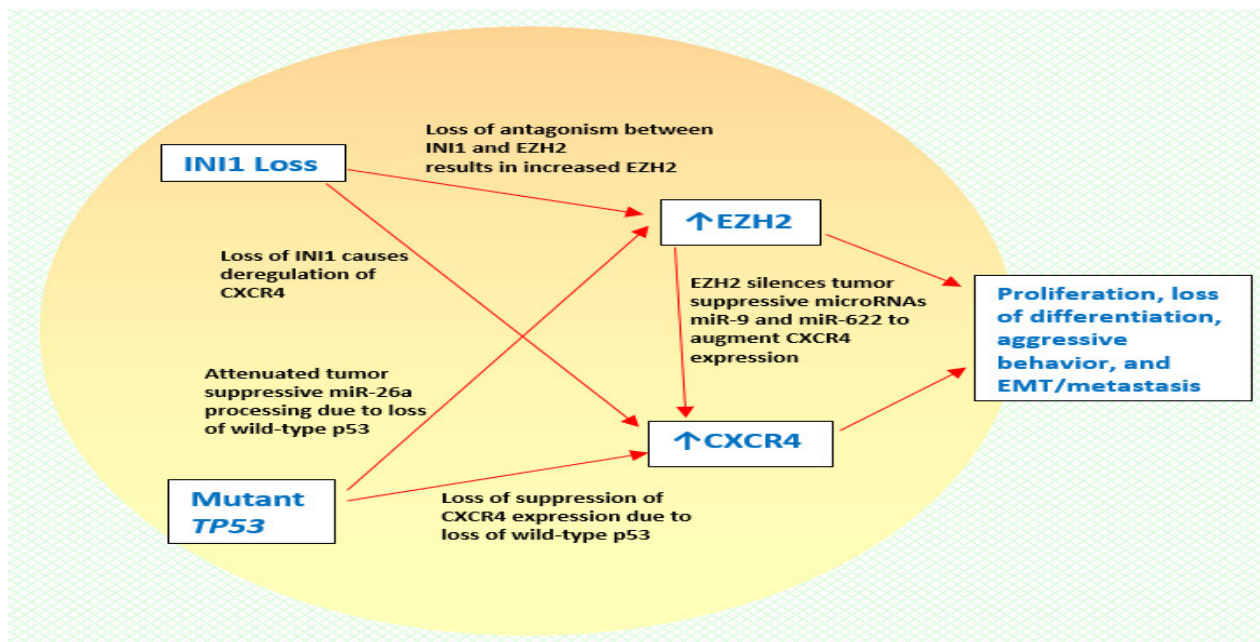


Figure 1. The graphical illustration of the INI1, EZH2, CXCR4, and mutant TP53 interaction.

2. Materials and Methods

The patient is a middle-aged man with a history of sacrococcygeal chordoma, status post-resection and radiotherapy five years ago. Post-surgery was complicated with neurologic deficits, a neurogenic bladder, and multiple wound infections necessitating a prolonged course of antibiotic therapy and surgical debridement. This time, the patient presented with severe intractable left-lower back pain radiating to the left leg; he was

unresponsive to conservative management, with an inability to ambulate and drainage from his previous surgical wounds. Also, he was found to have new hepatic, lung, and adrenal lesions, which prompted hospital admission and biopsy of the liver lesion.

The main author already knew about the antagonism between the SNI/SWF (which contains INI1) and EZH2 [7], and the ramifications of a *p53* mutation, including the induction of EZH2 expression due to the loss of the processing of miR-26a [13] and the loss of the negative regulation of CXCR4 by *p53* in its wild-type form [14]. Therefore, we set out to correlate the immunohistochemical findings with the genomic findings to test our theory that these markers of aggressive behavior (namely, EZH2 and CXCR4) would be upregulated in the patient's tumor due to the identified genomic alterations. Unstained sections prepared from the cell-block material of the patient's liver biopsy were used. The formalin-fixed paraffin-embedded (FFPE) tissue was stained with antibodies anti-*p53* (DO-7) primary antibody (Ventana[®], Oro Valley, AZ, USA), anti-Brachyury/Bry antibody [EPR18113] (Abcam[®], Cambridge, UK), anti-SNF5/SMARCB1 antibody [ERP20189] (Abcam[®]), anti-CXCR4 antibody [UMB2] (Abcam[®]), and anti-EZH antibody (Cell Signaling Technology[®], Danvers, MA, USA). Protocol was followed as per the insert for each antibody. The anti-*p53* (DO-7) primary antibody (Ventana[®]) is a prediluted mouse monoclonal antibody, in which the cell conditioning 1 standard (CC1) is used for the antigen unmasking, alongside a VIEW DAB detection kit. The anti-Brachyury/Bry antibody [EPR18113], anti-SNF5/SMARCB1 [ERP20189] (dilution 1:400), and anti-CXCR4 antibody [UMB2] (dilution 1:100) (all Abcam[®]) are rabbit monoclonal antibodies, in which heat-mediated antigen retrieval with Tris/EDTA buffer pH 9.0 and a mouse HRP polymer detection kit is utilized. The same goes for anti-EZH antibody (Cell Signaling Technology[®]) (dilution 1:100), but with EDTA buffer pH 8.0. Slides were then examined by bright-field microscopy to assess the staining intensity for each immunohistochemical marker. The results are discussed below.

3. Results

Imaging revealed multiple new hepatic lesions (Figures 2 and 3), bilateral pulmonary nodules, and a new 2.9-cm left adrenal nodule, favoring a diagnosis of a metastatic tumor. The patient was admitted to the hospital for a higher level of care.

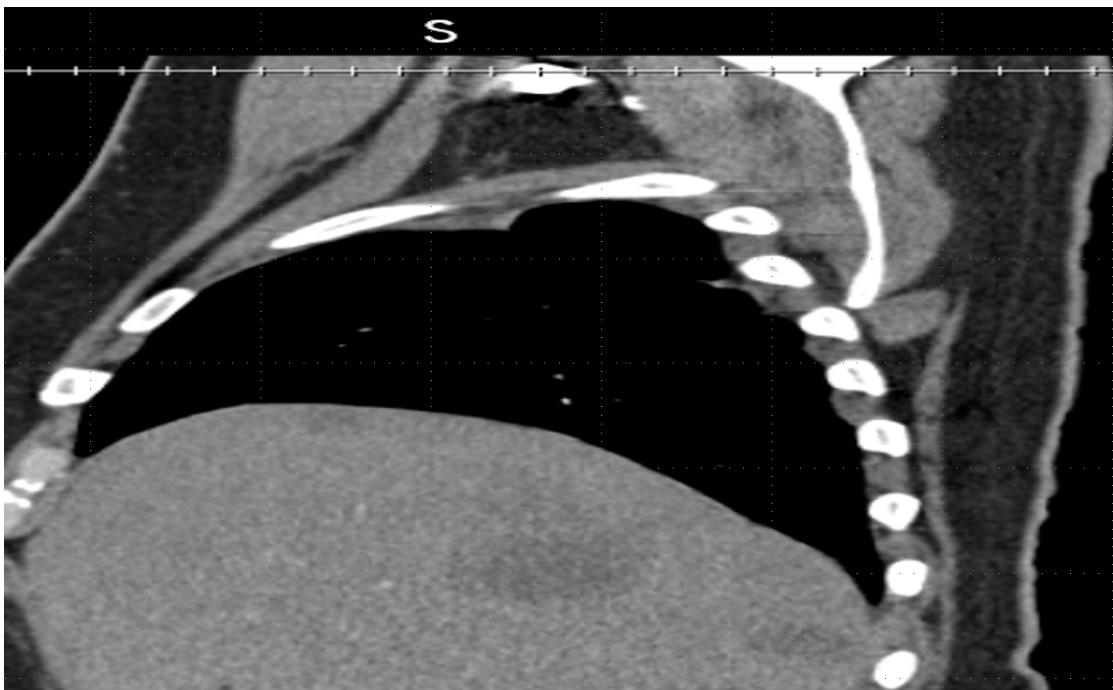


Figure 2. Sagittal Computed tomography imaging revealed multiple new hepatic lesions.

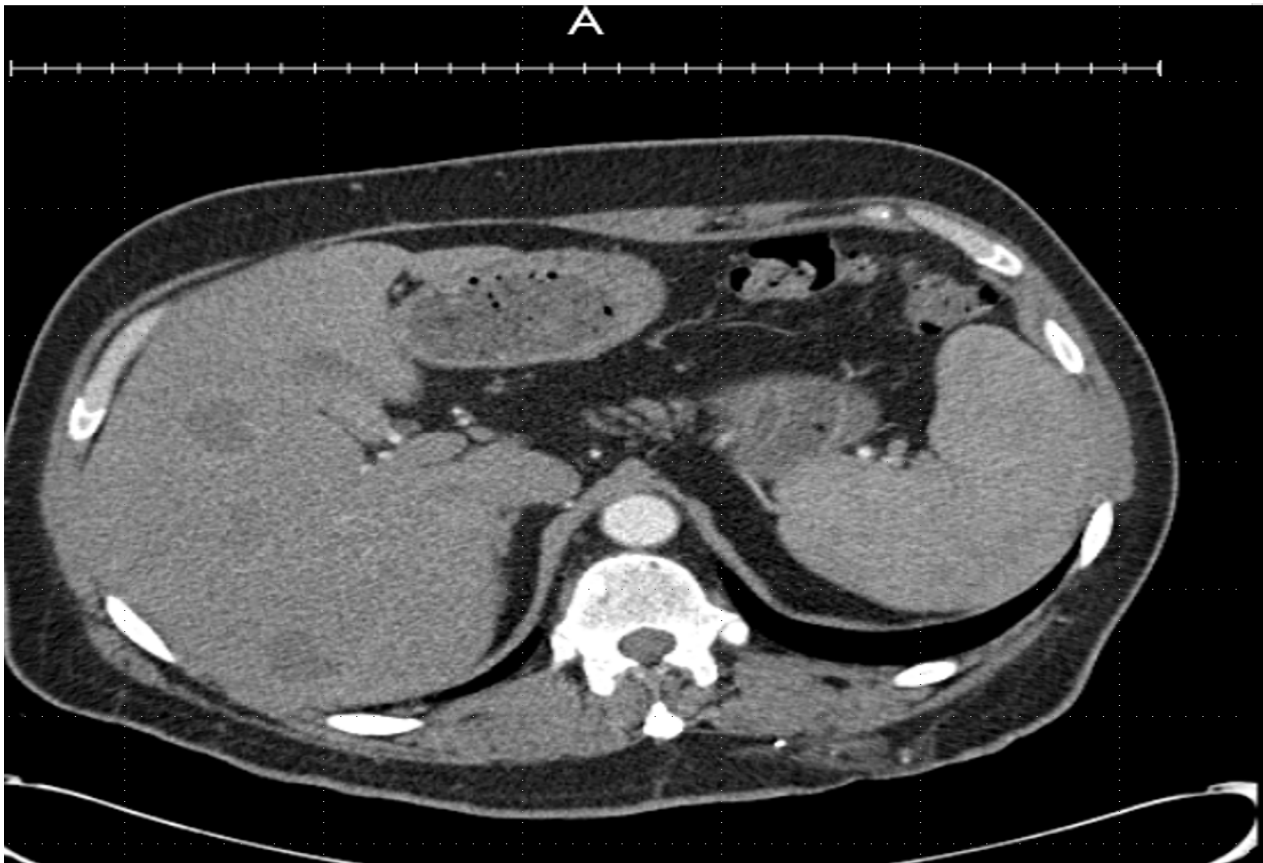


Figure 3. Coronal Computed tomography imaging showing multiple new hepatic lesions.

Laboratory results at the time of admission showed elevated CA-125 (231.5 unit/mL), alkaline phosphatase (290 Unit/L), lactate dehydrogenase (491 unit/L), and β 2-microglobulin (5 mg/L), along with a decreased albumin level (2.7 gm/dL). Other tumor markers (CEA, CA19-9, AFP) and liver function tests (aspartate aminotransferase, alanine aminotransferase, and total bilirubin) were within normal limits. The viral hepatitis panel was negative.

The clinical team decided to perform an ultrasound-guided fine-needle aspiration and biopsy of one of the liver lesions. Touch preparation (Figure 4: DiffQuick, 200X power field) and the biopsy (Figure 5: H&E, 100X power field) showed sheets of malignant epithelioid cells with a high nuclear-to-cytoplasmic ratio, vacuolated eosinophilic cytoplasm, areas of necrosis (Figure 6: H&E, 400X power field), and up to five mitoses per one high-power field (Figure 7: H&E, 400X power field).

An extensive panel of immunohistochemical markers was used to identify the origin of the hepatic lesion. The tumor cells were positive for Cam5.2, EMA, and CD56. The Brachyury immunostaining (Figure 8) was performed due to the patient's previous history and was positive. Additional markers were performed, and the tumor showed a Ki-67 proliferation index of approximately 80% (Figure 8), mutant p53 protein with diffuse and strong staining (Figure 8), and loss of INI1 (Figure 8), which had positive staining of internal controls such as entrapped hepatocytes and some inflammatory cells. Further to this, due to the aggressive biological behavior of the tumor, we tested for prometastatic CXCR4, which is a chemokine receptor, and the histone methyltransferase EZH2. The tumor showed a strong expression of both CXCR4 (Figure 8) and EZH2 (Figure 8). Tissue from the liver biopsy was sent for genomic testing, which showed a *SMARCB1* mutation, *TP53* mutation, and *RB1* loss in tumor cells.

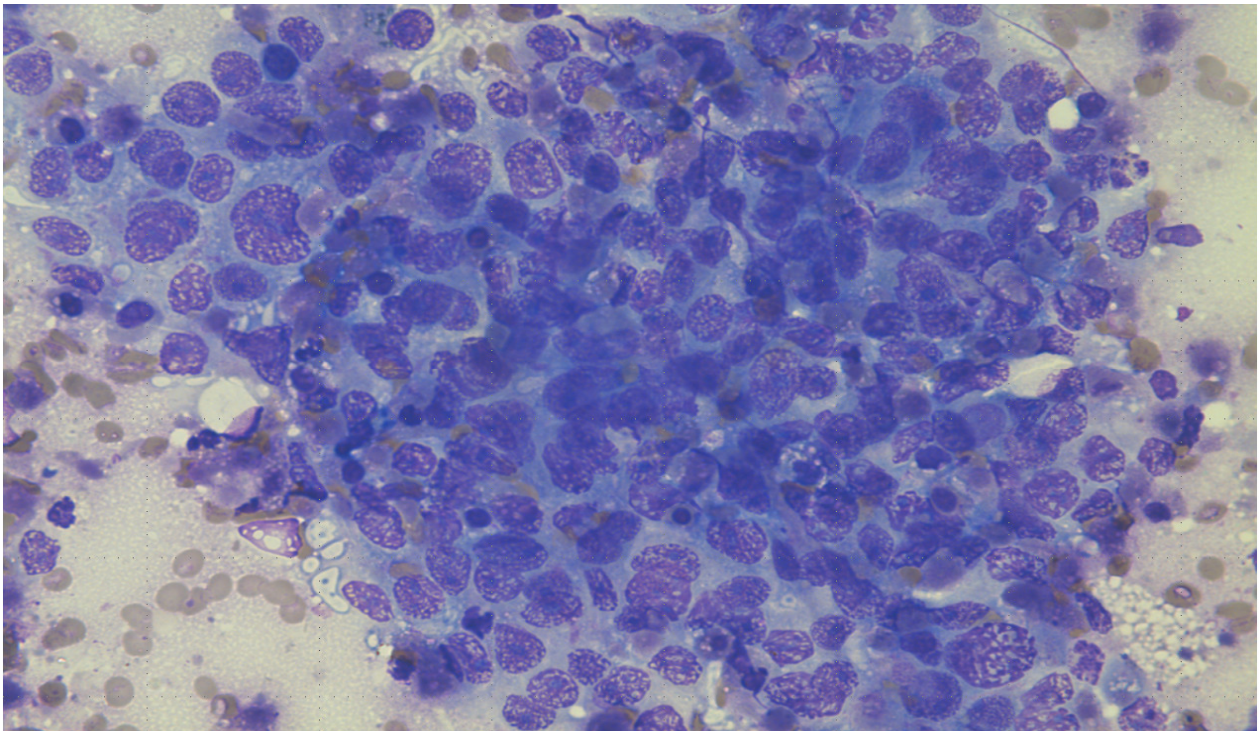


Figure 4. DiffQuick, 200X. The touch preparation of the ultrasound-guided fine-needle aspiration and biopsy of one of the liver lesions showing sheets of malignant epithelioid cells with a high nuclear-to-cytoplasmic ratio.

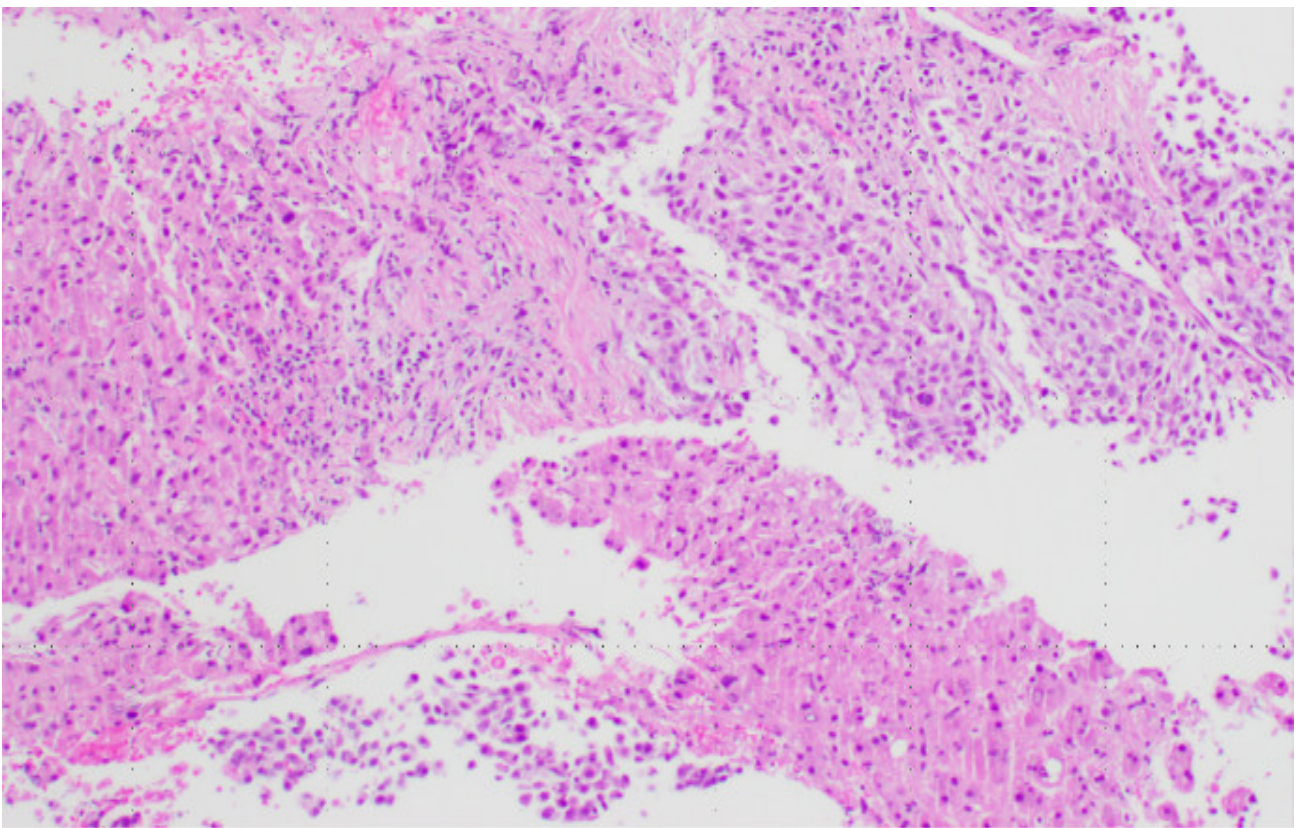


Figure 5. H&E, 100X. Ultrasound-guided fine-needle aspiration and biopsy of one of the liver lesions with sheets of malignant epithelioid cells.

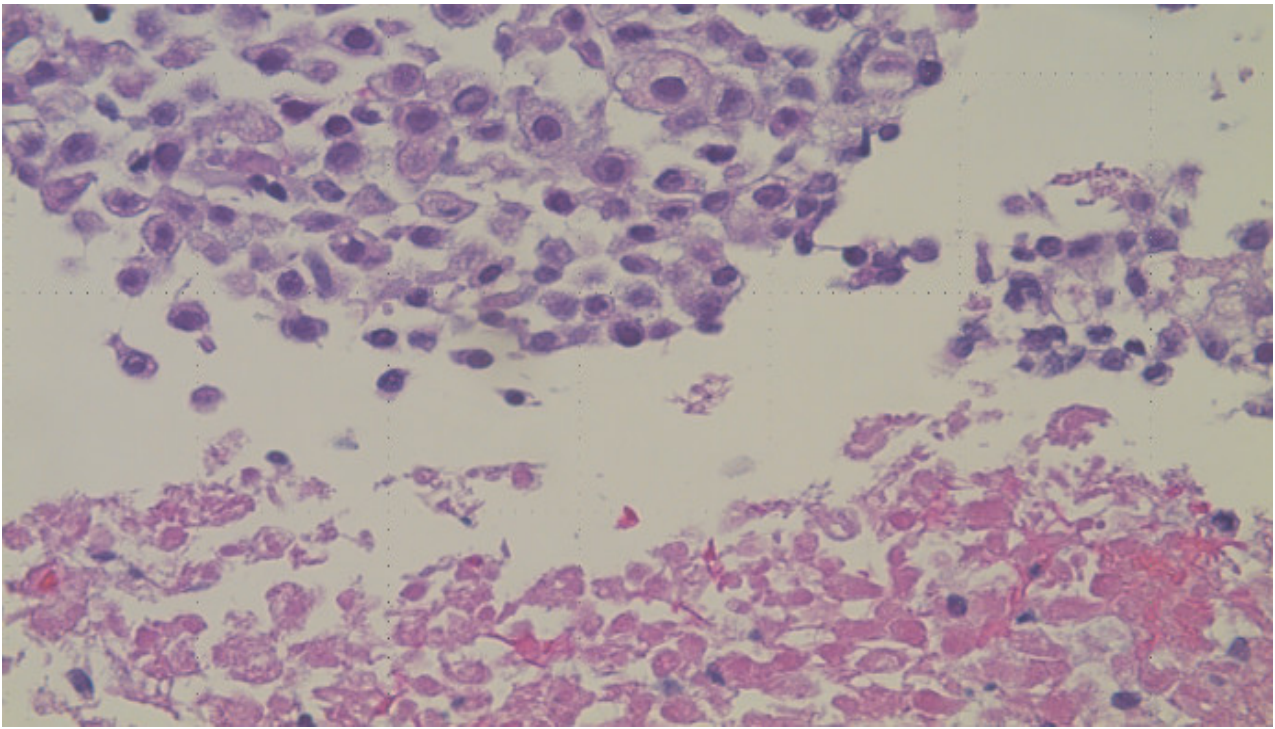


Figure 6. H&E, 400X. Sheets of malignant epithelioid cells (**top**) with a high nuclear-to-cytoplasmic ratio, vacuolated eosinophilic cytoplasm, and areas of tumor cell necrosis (**bottom**).

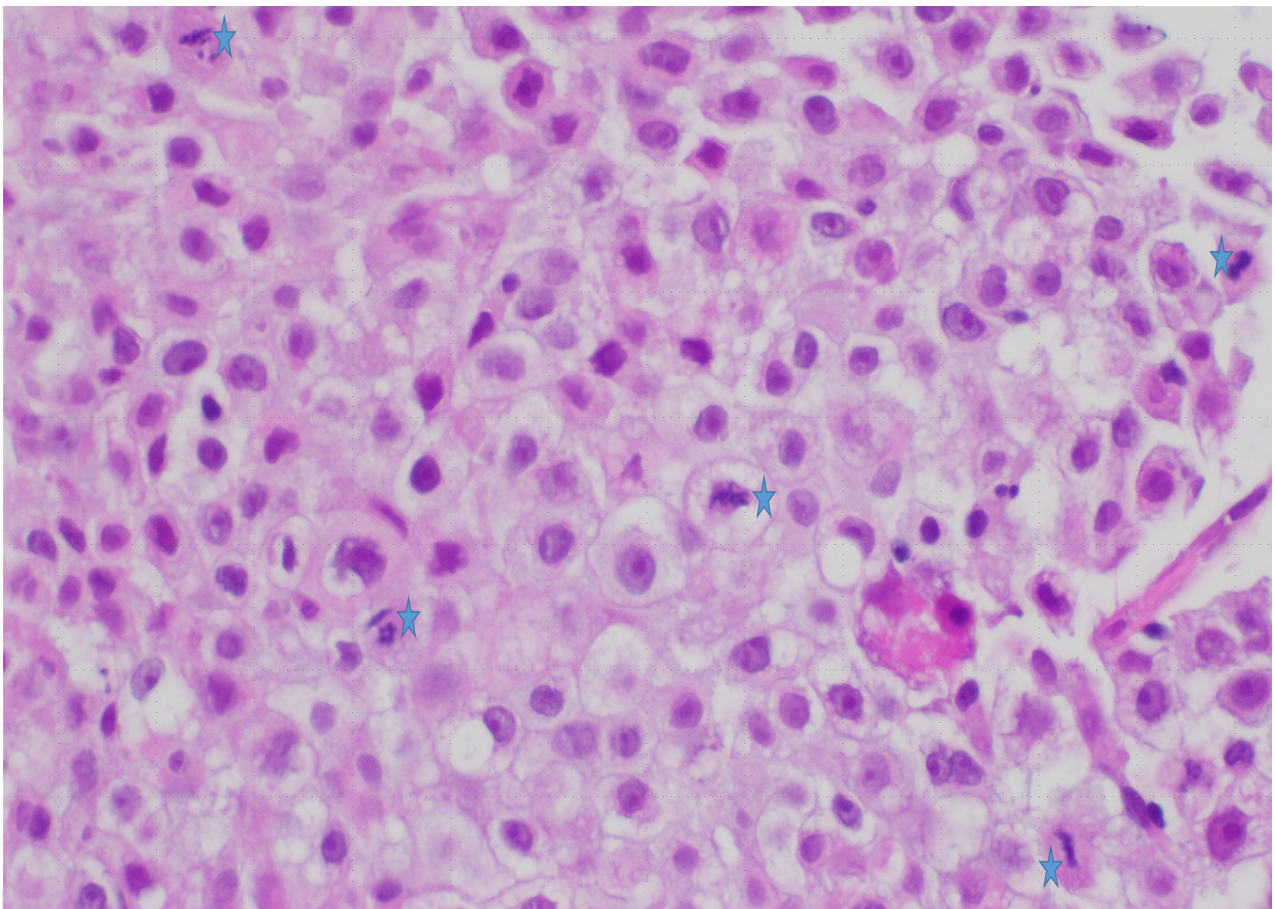


Figure 7. H&E, 400X. Tumor cells have up to five mitotic figures (**blue star**) per one high-power field.

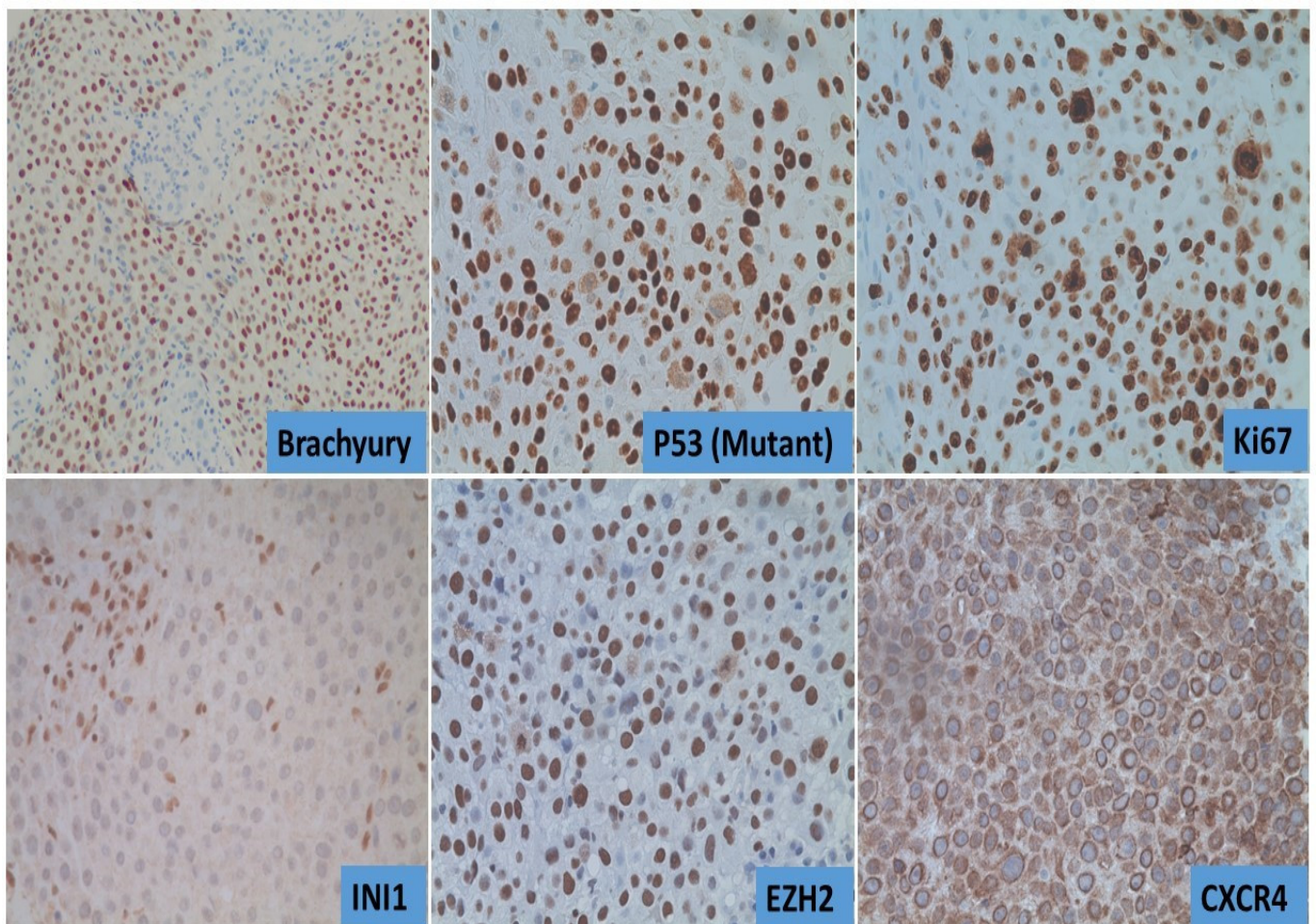


Figure 8. Immunohistochemical staining results of liver lesion biopsy: tumor cells are strongly positive for Brachyury (nuclear), EZH2 (nuclear), CXCR4 (cytoplasmic), and P53 (overexpressed, nuclear). INI1 is negative in tumor cells with positive internal control cells. The Ki67 proliferation index is very high in tumor cells (80%).

Immunohistochemical stains and genomic studies of the liver lesion supported a diagnosis of metastatic, poorly differentiated chordoma, which most likely represented malignant transformation of the patient's prior conventional sacrococcygeal chordoma. This is an uncommon phenomenon and represents a rare case with *SMARCB1/INI1* loss, a concurrent *TP53* mutation, and *Rb1* loss that most likely arose from malignant transformation of the patient's conventional chordoma.

It is important to identify this entity. Of course, in our case, the history was important, but a wide profile of immunohistochemical stains was performed before brachyury. Our knowledge and the experience gained while working up the case will help us to identify it more readily in the future. This tumor should not be confused with dedifferentiated chordoma; the characteristics of both dedifferentiated chordoma and poorly differentiated chordoma will be reviewed in the discussion section.

4. Discussion

The current World Health Organization (WHO) "Classification of Soft Tissues and Bone" classifies chordoma into three subtypes: conventional, chondroid, and dedifferentiated [16].

Conventional chordoma represents ~95% of cases of chordomas and is a locally aggressive neuraxial tumor. Conventional chordoma develops from ectopic remnants of the notochord and is thus considered to result from abnormal notochordal development [1].

It is usually diagnosed during the fourth to eighth decades of life, affecting men more frequently than women [17]. Most frequently, chordoma involves the sacrum (50%), though 35% involve the skull base and 15% affect the mobile spine. On radiologic imaging, chordoma will display destructive and lytic lesions, invariably extending into soft tissues, forming a sizable mass [17]. Macroscopically, it is a mass with a soft, tan-gray, gelatinous, and lobulated cut surface, and there are well-delineated borders with surrounding tissues. Histologically, conventional chordoma is composed of large epithelioid cells arranged in cohesive nests and cords with abundant eosinophilic cytoplasm and intracytoplasmic vacuoles imparting a bubbly appearance (physaliphorous). The extracellular matrix is myxoid, frothy, and basophilic. It usually has low mitotic activity with no tumor necrosis. Immunohistochemically, conventional chordoma typically expresses epithelial markers (keratin and EMA). The vast majority of conventional chordomas also stain for nuclear transcription factor T-brachyury and the majority stain with antibodies to the S100 protein [18]. Hsu et al. reported that knocking down brachyury in chordoma cell lines induces growth arrest and apoptosis [19], indicating that brachyury likely plays a role in the pathogenesis of these tumors. Resection of conventional chordoma is most often curative if the surgeon can achieve negative margins. Recurrences are not uncommon [2].

Chondroid chordoma is a rare variant and comprises only 4% of cases. These contain areas of conventional chordoma merging abruptly with regions resembling low-grade, hyaline-type chondrosarcoma. Neoplastic cells in chondroid chordoma are surrounded by a solid-appearing hyalinized matrix that mimics hyaline cartilage [20].

Dedifferentiated chordoma results from ongoing cumulative mutations in conventional chordoma. Dedifferentiated chordoma has a high-grade sarcoma component adjacent to conventional chordoma. However, one may or may not visualize a transitional area from a conventional chordoma. Dedifferentiated chordoma may be negative for S100, EMA, and brachyury, but is positive for vimentin and has a retained INI1. Dedifferentiated chordoma can have an aggressive clinical course and higher mortality than other subtypes [21], and can also have a mutation in *TP53* [22]. These two characteristics are further seen in the poorly differentiated chordoma (our diagnosis). To differentiate between the two entities, one should first look at the tumor morphology. While dedifferentiated chordoma most commonly has a sarcomatoid appearance, poorly differentiated chordoma is described as a more epithelioid-appearing malignancy. Poorly differentiated chordoma usually maintains brachyury expression and has the defining feature of INI1 loss, whereas dedifferentiated chordoma is usually negative for brachyury and has intact INI1 expression. Therefore, knowing the morphological, immunohistochemical, and molecular characteristics of both dedifferentiated chordoma and poorly differentiated chordoma, one should be able to confidently separate the two entities.

A newly recognized subtype of chordoma is poorly differentiated chordoma, which is more common in the pediatric age group and shows a more aggressive biologic behavior compared to other types of chordoma. A defining feature is the mutation in *SMARCB1*, which causes loss of INI1 expression in the immunohistochemistry, as in our reported case [2,23]. These tumors are not yet included as a distinct tumor entity in the WHO classification of soft tissue and bone tumors [16].

In poorly differentiated chordoma, the tumor cells are usually polygonal, with moderate to marked nuclear atypia, prominent nucleoli, an eosinophilic to vacuolated cytoplasm, and sometimes a rhabdoid morphology. Commonly, there is no extracellular myxoid matrix or physaliphorous appearance. Pronounced mitotic activity with areas of necrosis can present, as was seen in our patient [23].

5. Conclusions

Thus far, 53 cases of poorly differentiated chordoma with INI1 loss have been reported in the literature, most of which have occurred in the pediatric population and developed de novo [24]. However, our case occurred in an older patient after radiotherapy for a sacrococcygeal chordoma. This case of metastatic, poorly differentiated chordoma also

showed a concurrent *TP53* mutation, *SMARCB1/INI1* deficiency, and *RB1* loss, which resulted in malignant transformation of the patient's prior conventional chordoma, with loss of differentiation, cell cycle progression, and upregulation of prometastatic *CXCR4* and the histone methyltransferase *EZH2*, causing aggressive biologic behavior and metastasis. Recognition of this subtype and delineation from dedifferentiated chordoma are crucial since, compared to other chordoma subtypes, poorly differentiated chordoma has a significantly decreased mean overall survival and should be treated aggressively with multimodal therapy.

Author Contributions: All authors contributed to the original draft's preparation, its review and editing, drafting and revising it critically for important intellectual content, and in the final approval of the version to be published. All authors have read and agreed to the published version of the manuscript.

Funding: This research received no external funding.

Institutional Review Board Statement: Not relevant to this study.

Informed Consent Statement: Not applicable since we were not studying an intervention with care in this case and we did not look at outcomes or have endpoints. This is purely a genomic and immunohistochemical report of one case, where any information linked to the patient was de-identified and thus not relevant.

Data Availability Statement: Not applicable.

Conflicts of Interest: The authors declare no conflict of interest.

References

1. de Bree, K.; de Bakker, B.S.; Oostra, R.J. The development of the human notochord. *PLoS ONE* **2018**, *13*, e0205752. [[CrossRef](#)] [[PubMed](#)]
2. Lee, I.; Lee, R.J.; Fahim, D.K. Prognostic Factors and Survival Outcome in Patients with Chordoma in the United States: A Population-Based Analysis. *World Neurosurg.* **2017**, *104*, 346–355. [[CrossRef](#)] [[PubMed](#)]
3. Hasselblatt, M.; Thomas, C.; Hovestadt, V.; Schrimpf, D.; Johann, P.; Bens, S.; Oyen, F.; Peetz-Dienhart, S.; Crede, Y.; Wefers, A.; et al. Poorly differentiated chordoma with *SMARCB1/INI1* loss: A distinct molecular entity with dismal prognosis. *Acta Neuropathol.* **2016**, *132*, 149–151. [[CrossRef](#)] [[PubMed](#)]
4. Rekhi, B.; Michal, M.; Ergen, F.B.; Roy, P.; Puls, F.; Haugland, H.K.; Soylemezoglu, F.; Kosemehmetoglu, K. Poorly differentiated chordoma showing loss of *SMARCB1/INI1*: Clinicopathological and radiological spectrum of nine cases, including uncommon features of a relatively under-recognized entity. *Ann. Diagn. Pathol.* **2021**, *55*, 151809. [[CrossRef](#)] [[PubMed](#)]
5. Tirabosco, R.; Jacques, T.; Berisha, F.; Flanagan, A.M. Assessment of integrase interactor 1 (INI-1) expression in primary tumours of bone. *Histopathology* **2012**, *61*, 1245–1247. [[CrossRef](#)] [[PubMed](#)]
6. Mittal, P.; Roberts, C.W.M. The SWI/SNF complex in cancer-biology, biomarkers and therapy. *Nat. Rev. Clin. Oncol.* **2020**, *17*, 435–438. [[CrossRef](#)] [[PubMed](#)]
7. Raaphorst, F.M.; Meijer, C.J.; Fieret, E.; Blokzijl, T.; Mommers, E.; Buerger, H.; Packeisen, J.; Sewalt, R.A.; Ottet, A.P.; Van Diest, P.J. Poorly differentiated breast carcinoma is associated with increased expression of the human polycomb group *EZH2* gene. *Neoplasia* **2003**, *5*, 481–488. [[CrossRef](#)]
8. Wilson, B.G.; Wang, X.; Shen, X.; McKenna, E.S.; Lemieux, M.E.; Cho, Y.J.; Koellhoffer, E.C.; Pomeroy, S.L.; Orkin, S.H.; Roberts, C.W. Epigenetic antagonism between polycomb and SWI/SNF complexes during oncogenic transformation. *Cancer Cell* **2010**, *18*, 316–328. [[CrossRef](#)]
9. Sandgren, J.; Holm, S.; Marino, A.M.; Asmundsson, J.; Grillner, P.; Nistér, M.; de Ståhl, D.T. Whole exome and mRNA-sequencing of an AT/RT case reveals few somatic mutations and several deregulated signaling pathways in the context of *SMARCB1* deficiency. *Biomed. Res. Int.* **2015**, *2015*, 862039. [[CrossRef](#)]
10. Shi, Y.; Riese, D.J.; Shen, J. The role of the CXCL12/CXCR4/CXCR7 chemokine axis in cancer. *Front. Pharmacol.* **2020**, *11*, 574667. [[CrossRef](#)]
11. Liu, H.; Liu, Y.; Liu, W.; Zhang, W.; Xu, J. *EZH2*-mediated loss of miR-622 determines *CXCR4* activation in hepatocellular carcinoma. *Nat. Commun.* **2015**, *6*, 8494. [[CrossRef](#)] [[PubMed](#)]
12. Chien, Y.C.; Chen, J.N.; Chen, Y.H.; Chou, R.H.; Lee, H.C.; Yu, Y.L. Epigenetic silencing of miR-9 promotes migration and invasion by *EZH2* in glioblastoma cells. *Cancers* **2020**, *12*, 1781. [[CrossRef](#)] [[PubMed](#)]
13. Jiang, F.Z.; He, Y.Y.; Wang, H.H.; Zhang, H.L.; Zhang, J.; Yan, X.F.; Wang, X.J.; Che, Q.; Ke, J.Q.; Chen, Z.; et al. Mutant p53 induces *EZH2* expression and promotes epithelial-mesenchymal transition by disrupting p68-Drosha complex assembly and attenuating miR-26a processing. *Oncotarget* **2015**, *6*, 44660–44674. [[CrossRef](#)] [[PubMed](#)]

14. Mehta, S.A.; Christopherson, K.W.; Bhat-Nakshatri, P.; Goulet, R.J., Jr.; Broxmeyer, H.E.; Kopelovich, L.; Nakshatri, H. Negative regulation of chemokine receptor CXCR4 by tumor suppressor p53 in breast cancer cells: Implications of p53 mutation or isoform expression on breast cancer cell invasion. *Oncogene* **2007**, *26*, 3329–3337. [[CrossRef](#)]
15. Clarke, A.R. Murine models of neoplasia: Functional analysis of the tumor suppressor genes RB-1 and p53. *Cancer Metastasis Rev.* **1995**, *14*, 125–148. [[CrossRef](#)] [[PubMed](#)]
16. Fletcher, C.D.M.; Bridge, J.A.; Hogendoorn, P.C.W.; Mertens, F. *WHO Classification of Tumours of Soft Tissue and Bone Geneva*; WHO Press: Geneva, Switzerland, 2013.
17. Sebros, R.; DeLaney, T.; Hornicek, F.; Schwab, J.; Choy, E.; Nielsen, G.P.; Rosenthal, D.I. Differences in sex distribution, anatomic location and MR imaging appearance of pediatric compared to adult chordomas. *BMC Med. Imaging* **2016**, *16*, 53. [[CrossRef](#)]
18. Karpathiou, G.; Dumollard, J.M.; Dridi, M.; Dal Col, P.; Barral, F.G.; Boutonnat, J.; Peoc'h, M. Chordomas: A review with emphasis on their pathophysiology, pathology, molecular biology, and genetics. *Pathol. Res. Pract.* **2020**, *216*, 153089. [[CrossRef](#)]
19. Hsu, W.; Mohyeldin, A.; Shah, S.R.; Ap Rhys, C.M.; Johnson, L.F.; Sedora-Roman, N.I.; Kosztowski, T.A.; Awad, O.A.; McCarthy, E.F.; Loeb, D.M.; et al. Generation of chordoma cell line JHC7 and the identification of Brachyury as a novel molecular target. *J. Neurosurg.* **2011**, *115*, 760–769. [[CrossRef](#)]
20. Jeffery, P.B.; Biava, C.G.; Davis, R.L. Chondroid chordoma: A hyalinized chordoma without cartilaginous differentiation. *Am. J. Clin. Pathol.* **1995**, *103*, 271–279. [[CrossRef](#)]
21. Gong, L.H.; Liu, W.F.; Ding, Y.; Sun, X.Q.; Zhang, M.; Huang, X.Y. Dedifferentiated chordoma of the sacrococcygeal region: A clinicopathologic analysis and review of the literature. *Zhonghua Bing Li Xue Za Zhi* **2018**, *47*, 349–353.
22. Hung, Y.P.; Diaz-Perez, J.A.; Cote, G.M.; Wejde, J.; Schwab, J.H.; Nardi, V.; Chebib, I.A.; Deshpande, V.; Selig, M.K.; Bredella, M.A.; et al. Dedifferentiated chordoma: Clinicopathologic and molecular characteristics with integrative analysis. *Am. J. Surg. Pathol.* **2020**, *44*, 1213–1223. [[CrossRef](#)] [[PubMed](#)]
23. Shih, A.R.; Cote, G.M.; Chebib, I.; Choy, E.; DeLaney, T.; Deshpande, V.; Hornicek, F.J.; Miao, R.; Schwab, J.H.; Nielsen, G.P.; et al. Clinicopathologic characteristics of poorly differentiated chordoma. *Mod. Pathol.* **2018**, *31*, 1237–1245. [[CrossRef](#)] [[PubMed](#)]
24. Yeter, H.G.; Kosemehmetoglu, K.; Soylemezoglu, F. Poorly differentiated chordoma: Review of 53 cases. *APMIS* **2019**, *127*, 607–615. [[CrossRef](#)] [[PubMed](#)]